



HAL
open science

Performance of Notched Connectors for CLT-Concrete Composite Floors

Minh-Van Thai, Sylvain Menard, Sidi Mohammed Elachachi, Philippe Galimard

► **To cite this version:**

Minh-Van Thai, Sylvain Menard, Sidi Mohammed Elachachi, Philippe Galimard. Performance of Notched Connectors for CLT-Concrete Composite Floors. Buildings, 2020, 10 (7), pp.122. 10.3390/buildings10070122 . hal-03353129

HAL Id: hal-03353129

<https://hal.science/hal-03353129>

Submitted on 23 Sep 2021

HAL is a multi-disciplinary open access archive for the deposit and dissemination of scientific research documents, whether they are published or not. The documents may come from teaching and research institutions in France or abroad, or from public or private research centers.

L'archive ouverte pluridisciplinaire **HAL**, est destinée au dépôt et à la diffusion de documents scientifiques de niveau recherche, publiés ou non, émanant des établissements d'enseignement et de recherche français ou étrangers, des laboratoires publics ou privés.



Distributed under a Creative Commons Attribution 4.0 International License

Article

Performance of Notched Connectors for CLT-Concrete Composite Floors

Minh Van Thai ^{1,2,*}, Sylvain Ménard ¹, Sidi Mohammed Elachachi ² and Philippe Galimard ²

¹ Applied Sciences Department, University of Québec in Chicoutimi, Saguenay, QC G7H 2B1, Canada; sylvain_menard@uqac.ca

² Civil and Environmental Engineering Department, University of Bordeaux, 33000 Bordeaux, France; sidi-mohammed.elachachi@u-bordeaux.fr (S.M.E.); philippe.galimard@u-bordeaux.fr (P.G.)

* Correspondence: minh-van.thai1@uqac.ca

Received: 2 June 2020; Accepted: 4 July 2020; Published: 8 July 2020



Abstract: CLT-concrete composite floor systems are a solution for timber buildings with a long-span floor. It yields a reduction of carbon footprint and even eco-friendly structure at the end of its service life. This study will evaluate the structural performance of notched connectors in the CLT-concrete composite floor, comprised of the serviceability stiffness, maximum load, and behavior at failure. The parameters of the test plan are the loaded edge length, the notch depth, the concrete thickness, and the screw length. Other secondary variables are also assessed, such as different loading sequences, speed of test, and timber moisture content. Experimental results prove that the performance of the connector depends significantly but not linearly on the notch depth and the length of the loaded edge. The connector with a deeper notch and a shorter heel will be stiffer and more robust, but it also tends to have a brittle rupture. The test results also help validate a solution for deconstructable connector systems. A nonlinear finite element model of the connector is built and validated versus the experimental results. It yields reasonably good predictions in terms of resistance and can capture the load-slip relationship.

Keywords: shear test; CLT-concrete; notched connector; finite element model; deconstructable composite floor; timber-concrete composite floor; screw

1. Introduction

French engineer Pierre-Eugene Gauthier developed the idea of cross-laminated timber (CLT), then patented it in 1952 [1]. It was redeveloped in Austria in early 1990 [2] and saw much broader usage in Europe by the 2000s. CLT is particularly suitable for floor system applications. There have been many successful applications of CLT in the construction of mid-rise and high-rise buildings. Brock Commons (Vancouver, BC, Canada) is the highest only residential building in timber construction with 17 stories in CLT panels. Origine Project (Quebec City, QC, Canada) is a 12-story building based on a concrete podium, constructed using CLT panels and glued-laminated timber beams.

The idea of timber-concrete composite (TCC) was used for bridge structures in the 1940s and, recently, for the renovation of timber structures [3]. TCC has been an objective for many extensive studies regarding short-term [4], and long-term behavior [5,6], fire resistance performance [7], and prefabricated solutions [3,8]. These studies emphasized the advantages of the TCC solution: resistance and rigidity, but also fire and seismic resistance, easy and rapid installation, dry site, prefabrication capacity, acoustic and thermal isolation, environmental and in deconstruction. From an economic and environmental standpoint, TCC is an excellent balancing solution, rather than using an all reinforced concrete or all timber floor. CLT-concrete composite (CCC) structures inherit the advantage of a TCC one. In the case of mid- and high-rise buildings, CCC is notably more beneficial than a TCC system,

i.e., wooden beam–concrete slab, because we could lose up to 30 cm for each TCC floor as compared to a CCC one. This means one floor per 10 story building for a defined total height. The uses of CLT in timber-concrete composite structures are still in development. Though, there is a new successful application of the CCC at the Design Building, University of Massachusetts (Amherst, MA, USA). In this building, the floor span varied from 6 to 8 m, the floor section comprised a 175 mm of 5 ply CLT panel, 25 mm of rigid insulation, and 100 mm of reinforced concrete. The connector composite was the patented HBV system [9].

The connector system is the means to obtain the mentioned composite action. Since the timber-concrete connector would be deformable rather than infinitely stiff, the full composite section is impossible to achieve. Slip between timber and concrete layer results in a partial composite action. Many connector solutions for TCC are available, such as shear interlock, bolts, screw, metal plates [10]. They have been widely studied for four decades [11–14]. These solutions are all applicable for CCC structures; some require a few minor modifications. There were many recent studies dedicated to CCC structures, as well as their connector systems. Gerber [15] tested two types of connectors: screws, and HBV mesh, on timber-concrete composite panels (CLT, LVL, LSL). The study showed that the analytical expressions could reasonably predict dynamic properties. Mai et al. [16] conducted shear tests on the individual screw connectors and applied them to the full-scale CLT-concrete beams. The authors observed a higher dynamic and static performance on composite structure than on bare CLT floor [17]. In the Oregon State University report [18], Higgins et al. carried out short-term and long-term tests on a full-scale CLT-concrete composite floor. They found that HBV mesh possesses a superior performance. Recently, Jiang and Crocetti [19] studied the performance of a single notched connector and a full-scale CLT-concrete beam. Lag screws and steel stirrup reinforced the notched connectors. The authors confirmed that this type of solution is reliable, robust, stiff, and inexpensive.

Timber material has undeniable advantages in terms of carbon footprint; however, some sustainability issues remain when considering the end of service life. Since we opt for a composite solution due to the mentioned reasons, a TCC floor with permanent connector systems would spawn an amount of solid waste with an incredibly low possibility of reusing after the dismantling. This would cause a mixture of concrete and timber and hence make timber lose its environmental-friendly characteristic. Hence, an adaptation for the deconstructable connector will facilitate the dismantling of the CCC structure and enhance the reusability of materials [20].

In this study, we conducted a shear test on a reinforced notched connector of CCC structures. The main objectives are to investigate and compare the influence of many variables on the load-bearing capacity, the stiffness modulus, and the post-peak behavior that could be associated in some way to its ductility. The solution of a deconstructable connector for CCC structures is proposed and tested. A finite element model was also built in this study to understand the involved mechanisms, and the experimental result would validate this model.

2. Specimen Geometry and Material

2.1. Materials Properties

The CLT material used in this study, provided by Nordic Structures® (Montréal, QC, Canada), was a 5-ply CLT and had a thickness of 175 mm. Its lamella configuration is 35L-35T-35L-35T-35L, where “35” is the thickness in mm while “L” and “T” are the longitudinal and transversal directions, respectively. The timber specimens were E1 grade, complying with the standard ANSI/APA PRG-320-2019 [21]. E1 grade CLT should have 1950f-1.7E (the term “1950f-1.7E” represents the bending stress parallel to grain, 1950 lb/in², and the modulus of elasticity, 1.7×10^6 lb/in²) Spruce-pine-fir MSR lumber in all parallel (longitudinal) layers and No. 3 Spruce-pine-fir lumber in all perpendicular (transversal) layers. The panel was face-glued by Purbond HD E202 adhesive (Henkel Canada Corporation, Mississauga, ON, Canada) and not edge-glued [22]. Table 1 presents the characteristic values of the CLT material.

Table 1. Properties of CLT and concrete.

Property	Unit	CLT Longitudinal Layer *	CLT Transversal Layer *	Concrete **
Compression strength, f_c	MPa	23.6	8.5	36.8
Modulus of elasticity, E	GPa	11.7	9.0	22.3
Density	kg/m ³	514	514	2262

* Standard properties of CLT given by the manufacturer [22]. ** Experimentally measured on five cylindrical specimens according to the ASTM C39/C39M—18 standard [23].

After each shear test, moisture content of the timber was measured at six different randomly chosen locations on the two sides of the CLT part. The average moisture content of all tested specimens had a mean of 15.7%, with a coefficient of variation (CoV) of 14%. The high moisture content of the wood is because the specimens were stored in an uncontrolled environment, and the measurement technique only allowed sampling up to 1 cm from the timber surface.

The humidity exchange between timber and concrete is an open-ended question. Roughly speaking, if the timber absorbs water too much from concrete or vice versa, the stiffness and strength of both materials will be affected [24]. Polyethylene film was considered in the design since our knowledge of the humidity exchange between timber and concrete is limited for the case of CLT-concrete; hence, an unknown variable. Humidity isolation, in this case, is necessary. The thickness of the crystal polyethylene film was about 50 μm (Figure 1a). This film would also reduce a certain amount of friction between timber and concrete and compensate for the phenomenon of eccentricity. In the full-scale floor, this friction phenomenon is minor, and therefore the necessity of this layer lies in its capacity of humidity isolation. For an application on-site, once we control this unknown variable, the removal of this film (if it is a case) would not cause any significant difference between the laboratory test and real behavior.

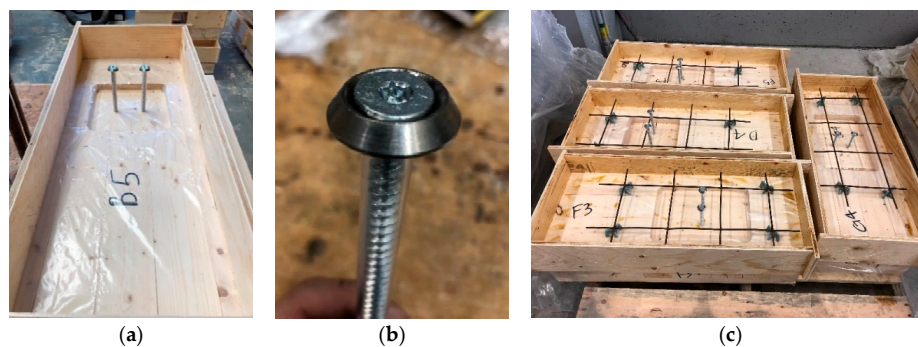


Figure 1. Specimen with preinstalled polyethylene film (a), vertical attachment part with a threaded screw, counter-sunk washer and plastic sleeve installed (b), reinforcing steel mat of the specimens (c).

A local supplier provided the concrete material with the indicated class of C35. The nominal aggregate size was 14 mm to assure a complete fill of concrete in the minimum notch's depth of 20 mm. There was also water-reducing admixture in the mix to achieve the same objective. Standard ASTM C39 [23], the test method for compressive strength of cylindrical concrete specimens, was used for the measurements of the compression strength and the modulus of elasticity of concrete. The last column of Table 1 indicates the properties of the concrete material. To prevent the uplift phenomenon, screws or bolts were adopted as the vertical attachment [19]. For deconstructable composite floors, these screws must be easy to uninstall. According to Gutkowski et al. [25], some adjustments were made to simplify the implementation. The vertical attachment systems comprised a screw, a plastic sleeve, and a washer (Figure 1b). ASSY VG countersunk head screws (My-Ti-Con Ltd., Surrey, BC, Canada), with a diameter of 8 mm and full-length threaded, were used in the tests. They had an identical outer diameter and facilitated the installation of the sleeve. A 90° washer put on each screw head was to

compensate for the bearing load lost due to the sleeve. The head of the screw was at the same level as the top surface of the concrete layer. The plastic sleeve prevented contact between the screws and the concrete. This solution provided easy access to the head of the screw to uninstall it.

2.2. Test Specimens

The “connector” is the zone that transfers the force from one material to another. The “connector” term in this study was used interchangeably with the “connector system,” which implied the assembly of the timber female part, the male concrete part, and screws.

CLT panels of 175 mm thickness were all cut into pieces with a dimension of 300 mm by 750 mm. A rectangular notch was then cut into the CLT specimen by using a round drill bit. The four corners of the notch were round at the radius of 20 mm. The concrete layer had a thickness of 80 mm or 100 mm. In this study, the part in front of the loaded edge was called the heel of the connector. This is the timber part that supported the compression and shear force transferred from the male concrete part. In our study, the heel part usually comprised more than two lamellas and the round edge of the loaded side. Heel length had three possible levels: 300, 350, and 400 mm. Notch depth varied in three-level: 20, 25, and 35 mm, without exceeding the maximum thickness of the first CLT layer. Two self-tapping screws reinforced each connector. The length of the screw was 160 mm or 220 mm. A reinforcing steel mat of 150 mm of the square spacing and a diameter of 6 mm were put in place to prevent a premature crack in concrete due to shrinkage. Sixty specimens were distributed into thirteen series and tested in two phases, the first phase comprised of eight series from A to H, and five series from I to M in the second phase. Table 2 and Figure 2 present the detailed parameters of each series.

Table 2. Parameters of test series, in mm.

Serie	No. of Specimens	Heel Length (a) in mm	Notch Depth (b) in mm	Screw Length (c) in mm	Concrete Thickness (d) in mm
A	5	400	20	160	80
B	5	400	20	220	100
C	5	400	35	160	100
D	5	400	35	220	80
E	5	300	20	160	100
F	5	300	20	220	80
G	5	300	35	160	80
H	5	300	35	220	100
I	6	400	25	220	80
J	3	300	25	220	80
K	3	350	20	220	80
L	3	350	35	220	80
M	5	350	25	220	80

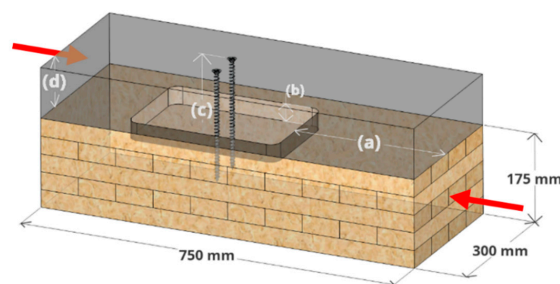


Figure 2. Diagram of a typical specimen, with indicated (a) heel length, (b) notch depth, (c) screw length, (d) concrete thickness.

Many variables were considered for the experimental plan. They were the design dimension one of the notched connectors: the length of the heel part, the length, depth, width of the notch, and thickness of the timber and concrete layer:

- To study the influence of the screw and to validate the unscrewing option, the screw length was included in the plan.
- A study in the LVL-concrete individual notched connector [24] showed that the length of the notch is not a significant issue in terms of stiffness and strength.
- The aspect of eccentricity and the derived compression between timber-concrete was much related to the length of the heel part.
- The notch depth was a critical parameter since the characteristic of CLT is sensitive in the depth direction, i.e., one layer is perpendicular adjacent to the other.
- Since the notch depth was not exceeded the thickness of the first layer of the lamella, and the characteristic of this layer was uniform transversally. A fixed notch's width of 200 mm was chosen.
- The thickness of the concrete layer was included in the testing plan. This variable was to verify the influence of the eccentricity (between axial force in timber and in concrete).
- We chose to use 5-ply-CLT and hence fixed the thickness of the timber layer to 175 mm. This is because a thinner (three plies) or thicker (seven plies) CLT would not be suitable for our future application of long-span composite floor systems (~9 m span).

2.3. Test Setups

The configuration adopted for the shear test is an asymmetrical specimen system. This type of configuration was cheaper to fabricate than the symmetrical one, and a more significant number of the specimens could be tested. The difference is that the asymmetrical test would estimate the shear stiffness and strength higher than the symmetrical one [12]. The eccentricity moment occurred when the testing machine applied on the timber part; this would generate compression force and hence the friction between timber and concrete on the upper part of the specimen [11]. For TCC connector systems, Lukaszewska [11] estimated that the stiffness and strength difference between an asymmetric specimen and a symmetric one was about 10%, depending on the specimen dimensions. In this study, since there was a thin polyethylene film at the material interface, the effect of this phenomenon might be lessened.

The bench adaptor comprised of two I-profiles welded perpendicular to each other. The specimen was placed on a fixed metal plate, only by the concrete part. The moving part of the testing machine transferred the load on a metal plate, then distributed the charge to the timber part of the specimen. Teflon plate was put on the vertical I-profile to reduce the friction between the sample and the I-profile (Figure 3). The testing machine, driven by a defined displacement rate, could produce a maximum charge of about 445 kN.

Two analog laser sensors (ALSs), were fixed on two sides of the sample to capture the relative displacements between the two layers. The ALSs were fixed on the timber part by screws. The install area of the two ALSs was at about 150 cm to the edge of the sample. This location was where the loaded edge of the notched commences. The ALSs were connected to amplifier units before transmitting the data to the computer. Another displacement sensor was integrated into the testing machine to measure the total displacement of the timber part. The vertical charge applied to the specimen was measured by a sensor of the testing machine.

Standard EN 26891 [26] proposed a protocol for the determination of resistance characteristics of the timber connector subjected to static loading. The total time for testing was about 15 minutes. The condition for the ending of the test was whether the charge has a significant drop, or the relative displacement reached 15 mm. We used a customized forklift to put the specimen into the bench adaptor. Once the sample was in place and well-positioned, the speed test was set by turning the dial manually. The loading speed of the test was averagely 1.3 mm per minute, and it varied greatly due

to manual handling. However, with the order of magnitude of loading speed, the result shows no correlation between it and the stiffness or the resistance. After the tests, we measured the moisture content and then dismantled some specimens for further study. Specimen disassembling helped us get a closer look at the failure mechanism and define the type of failure.

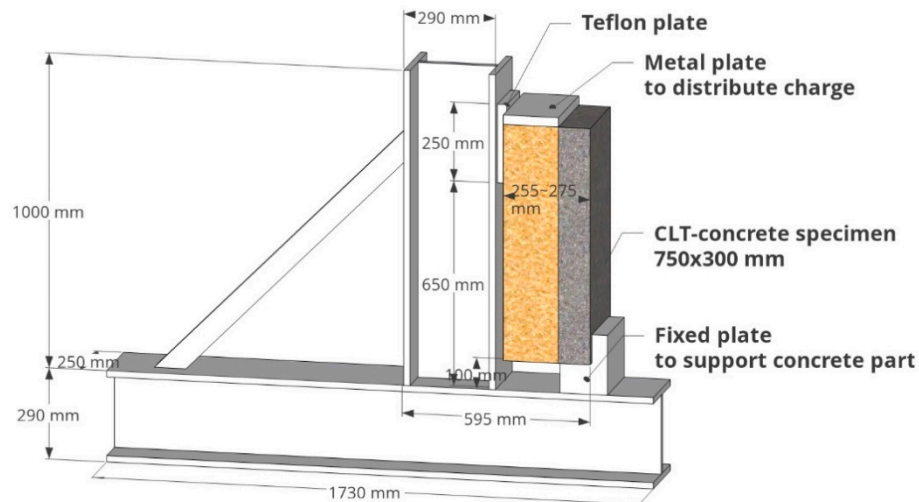


Figure 3. Adaptor for the asymmetrical CLT-concrete specimen.

According to Standard EN 26891, the slip modulus of the service state limit k_s is defined on the initial modified displacement, from 10% to 40% of the maximum load. This definition was proposed uniquely for the first loading sequence. The range from 0% to 10% of the maximum load comprised the very first loading sequence; the contacts between connector elements were not assured.

In this study, we used the notation K_1 and K_2 as the slip modulus of the first loading sequence and second loading sequence, respectively (Figure 4). By applying the linear regression $y = \beta y + \alpha$ on all the data points between the modified displacement, K_1 and K_2 were obtained as the slope of the regression line. The maximum load F_{max} was the load reached at the curve peak or 15 mm of displacement. Both K_1 and K_2 were defined over the range from 10% to 40% of the maximum load. The modulus K_1 had the same meaning as k_s , although we used the regression slope instead of an arbitrated displacement point for the determination of the modulus. In the other hand, K_2 had no counterpart in the standard in terms of physical meaning (modulus of second loading sequence). From our point of view, K_2 is more suitable for the calculation of vibration behavior.

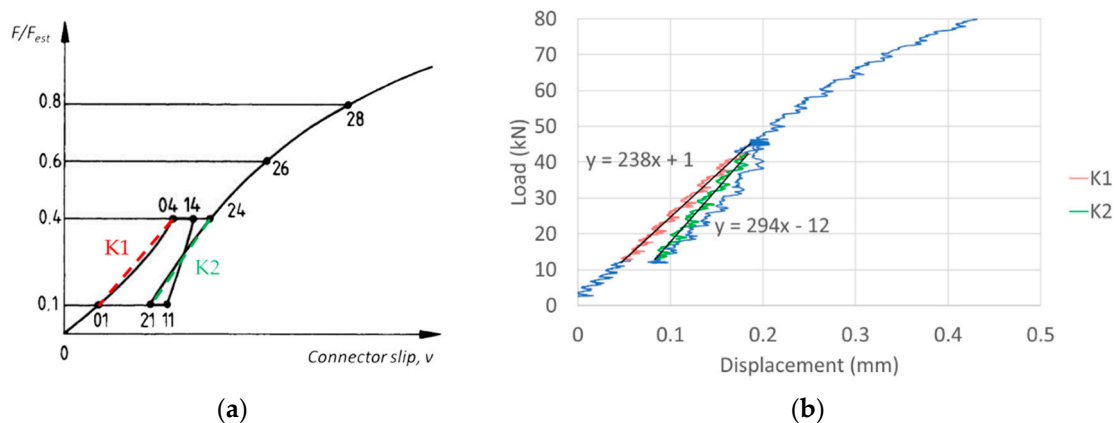


Figure 4. Theoretical loading procedure from EN 26891 (a) and stiffness K_1 (red) and K_2 (green) determination of specimen A2 (blue) on raw data representation (b).

3. Experimental Results and Discussion

3.1. Overview

Three different failure types were observed: ductile failure of the specimen due to the compression in the timber contact zone (type timber ductile - TD), brittle failure of the specimen due to the shearing-off of the timber lamellas in the heel (type timber brittle - TB). Furthermore, there was a combination of type TD and TB. The specimen had crushed timber and a part of its lamella sheared-off (type TD + TB). Brittle failure of the specimen due to the shear failure of the concrete part was noted as CB (type concrete brittle). The average stiffness and strength of the 13 series are presented in Table 3, with the corresponding coefficient of variation (CoV).

Table 3. Summary of tested series.

Series	K1		K2		F _{max}	
	Mean	CoV	Mean	CoV	Mean	CoV
	kN/mm	%	kN/mm	%	kN	%
A	224	13	294	5	127	10
B	213	18	303	15	140	9
C	248	8	311	8	221	5
D	238	12	315	5	221	11
E	199	16	258	7	140	4
F	202	4	256	6	151	7
G	208	9	274	11	211	7
H	195	19	254	13	217	9
I	242	13	326	13	177	4
J	208	1	286	7	169	5
K	202	1	270	13	158	7
L	205	7	291	17	238	6
M	212	12	311	14	175	10

As compared to the results of other studies [15,16,27,28], stiffness of the notched connector was on average higher than for the screw connector, but still far lower than HBV mesh. A pair of screws could have a shear stiffness that varies from 0.14 kN/mm² to 0.3 kN/mm², while that of HBV mesh was about 0.825 kN/mm². The experimental results of this study showed that the stiffness varied from 0.34 to 0.43 kN/mm². The unit kN/mm² indicates the shear stiffness (kN/mm) per connector length (mm). Figure 5 presents the load-displacement curves of 60 specimens distinguished by their series. The resistance varied from 108 kN to 253 kN depend on the notch geometry, especially the depth of the connector.

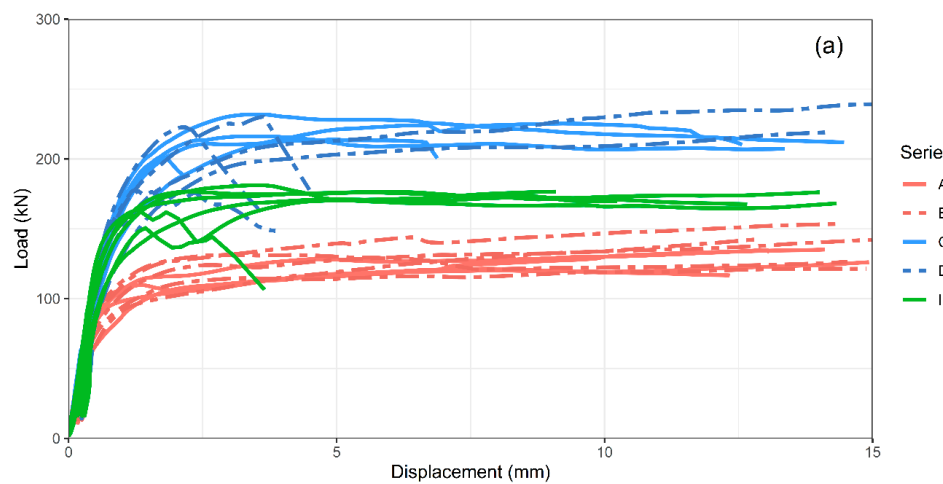


Figure 5. Cont.

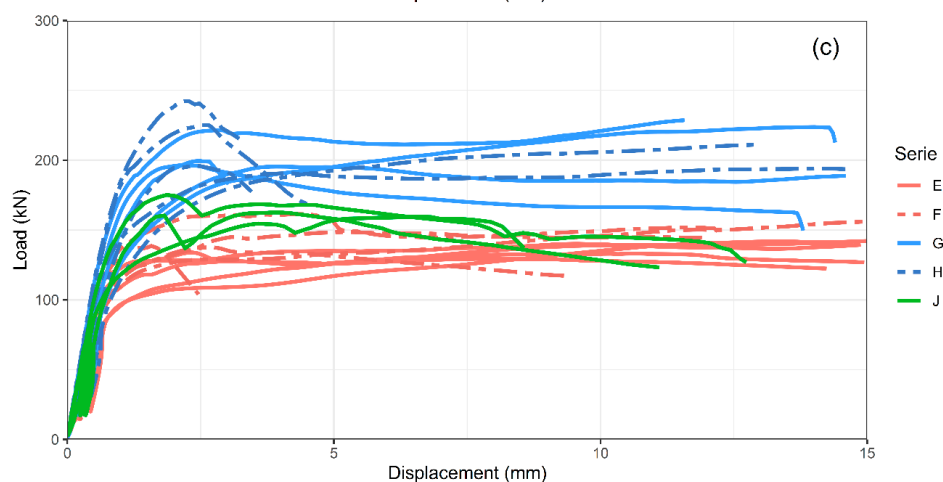
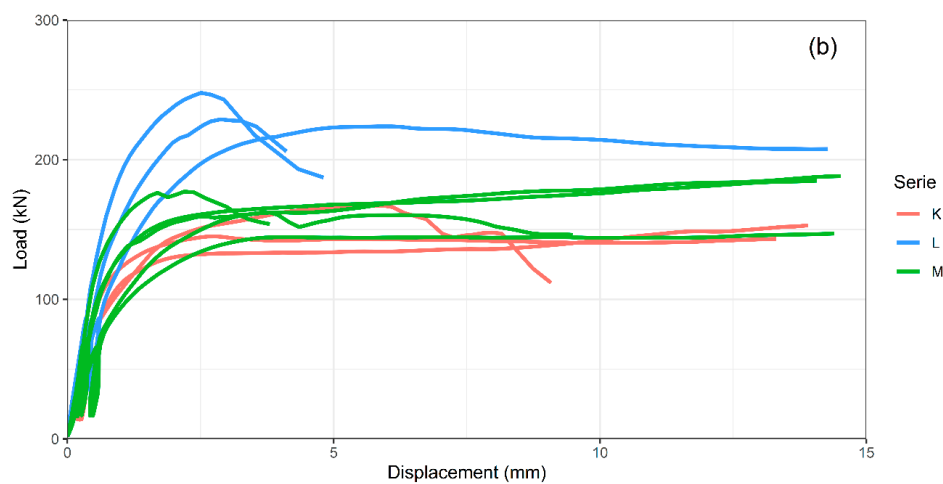


Figure 5. Load-displacement curves of specimens that have (a) 400 mm, (b) 350 mm, (c) 300 mm heel length, curves in red indicate 20 mm notch depth specimens, 25 mm in green, and 35 mm in blue.

There were distinct gaps between the curve family with the heel length of 400 mm (Figure 5a). However, the post-peak behavior was less consistent in other series of 350 mm and 300 mm heel length (Figures 5b and 6c). This is because the shorter heel length specimens have few materials to dissipate the charge and more likely sustain the timber softening.

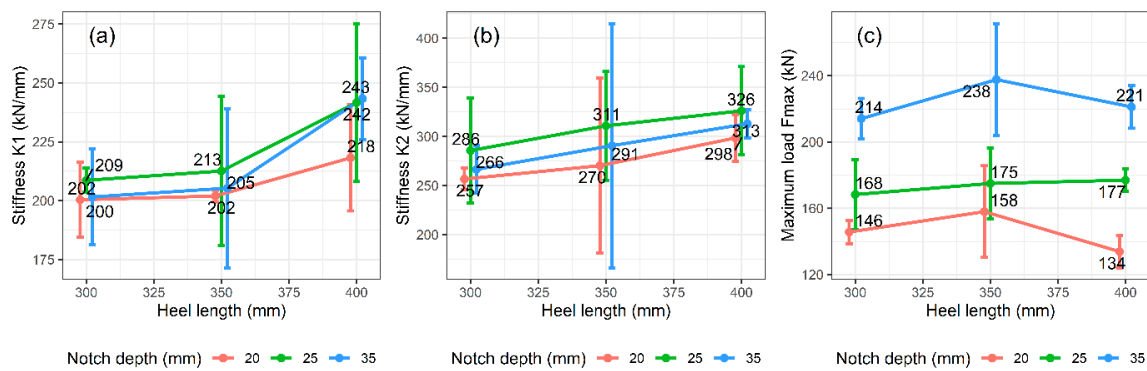


Figure 6. Stiffness K1 (a), K2 (b), and maximum load Fmax (c) of different notch depths.

3.2. Influence of Heel Length

Figure 6 exhibits the relationship between the heel length and the variables of interest, namely K1, K2, and Fmax. One can see an increase of about 15% of the stiffness K1, K2, when the heel length increases from 300 mm to 400 mm (Figure 6a,b). Heel length was assumed not to influence either the stiffness or strength of the connector. This slight increase was probably because of the asymmetrical properties of the test. The lengthy heel magnified the eccentricity and the friction between concrete and timber. The resistance of the connector of different notch depth distinguished clearly from each other's; they developed almost independently regarding their heel length. Modulus K2 was more consistent than K1 since the specimen was stabilized after the first loading sequence. In terms of the effect of heel length on the failure type, a specimen with shorter heel tended to have its lamellas sheared-off at failure. The error bars in the graphs represent the 95% confidence interval of the mean value \bar{x} . They are calculated as $\bar{x} \pm t_{n-1} \cdot s / \sqrt{n}$, with s is the standard deviation of the sample, n is the sample size, and t_{n-1} is the upper $(1 - 0.95)/2$ critical value for the t distribution with $(n - 1)$ degrees of freedom. Since the standard error was significant in some average data points, the evolution of stiffness K1, K2, was challenging to be verified.

3.3. Influence of Notch Depth

Figure 7a,b show the evolution of slip modulus when the notch depth increases. A deeper cut did not yield a stiffer connector. In most of the cases, the notch with 25 mm depth had the highest stiffness. In the notch with 35 mm of depth, the timber material of the first layer of the lamella was extracted entirely, and the second layer, which laid in the direction perpendicular to the first one, was weaker in terms of modulus perpendicular to the grain. The transversal timber lamellas were also not glued edgewise. They could be the reason for the "peak" trend of the slip modulus curves.

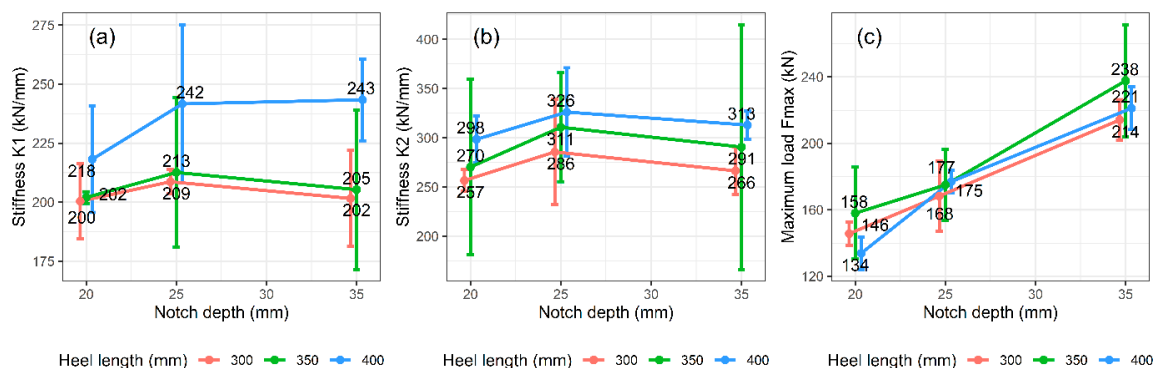


Figure 7. Stiffness K1 (a), K2 (b), and maximum load Fmax (c) of different heel lengths.

Figure 8a,b show the stiffness K1 and K2 per notch depth. The modulus gained per millimeter of notch depth was higher in the less deep notches. The shallow notch used the material more effectively in terms of stiffness, and further extraction of material in the topmost longitudinal layer would reduce the effectiveness of the connector. The linear correlations between the stiffness per depth and the notch depth were also observed.

The resistance of the connector is higher for the deeper cut (Figure 8c). An increase of the resistance of about 50% was observed when the cut more profound. The correlation between notch depth and the maximum load Fmax was almost linear. The notch depth had a more significant effect on maximum load, as compared to the effect of heel length in Figure 6c. The coefficient of variations of mean data points of the maximum load was considerably smaller than the other two responses (i.e., modulus K1 and K2). It meant that the experimental measurement of stiffness was difficult, and the maximum load of the notch would be more straightforward to be predicted by the variable of notch depth. A shallower notch connector tended to have the loaded edge crushed rather than the shear-off lamellas (cf. Section 3.7). Hence, the curves of these specimens had a more prolonged post-peak displacement that varied from 10 to 15 mm. Optimization of the notch depth will have to balance between the performance and the post-peak behavior.

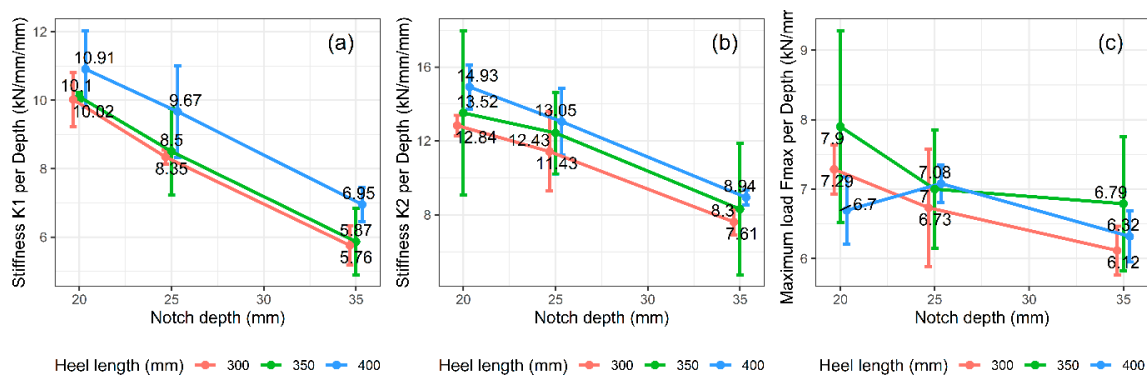


Figure 8. Stiffness K1 (a), K2 (b), and maximum load Fmax (c) per notch depth of different heel lengths.

For a CCC notched connector, Jiang et al. [19] reported a serviceability stiffness per 25 mm notch-depth of 15.3 kN/mm² and the resistance per depth of 7.1 kN/mm, while the corresponding results of our study were 12.5 kN/mm² and 7.0 kN/mm. The notch connectors in this study featured a round corner at the loaded edge while Jiang et al. tested a full-width square notch. This detail generated a transverse component of the applied force exerted on the notch. It might be the reason for the less stiff connector observed in this study.

3.4. Influence of Concrete Thickness and Screw Length

Figure 9 shows some minor changes (about 10% maximum) of the stiffnesses and the resistance of the connector in terms of concrete thickness and screw length. It could be concluded that these two variables do not influence the overall performance of individual notch connectors. Since the implementation of the deconstructable screw part yielded no difference in terms of the structural performance of the connector, this solution was possible for CLT-concrete floors systems. The uninstalling of the screws was carried out without any difficulty (Figure 10) by using a wired screwdriver.

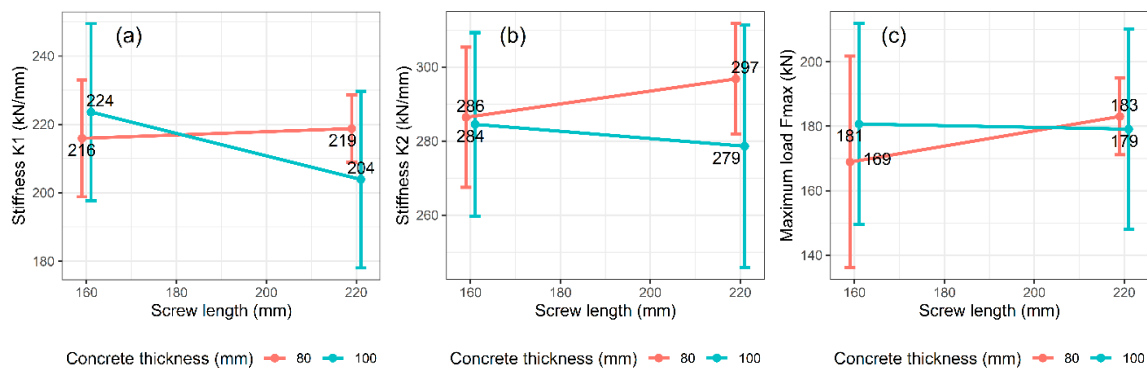


Figure 9. Stiffness K1 (a), K2 (b), and maximum load Fmax (c) in terms of screw length and concrete thickness.

3.5. Influence of Loading Sequence

The modulus of the second loading sequence K2 was on average 35% higher than for K1. This is because the contact between the component of the connector was well established after the first loading sequence. Any possible gaps between them were closed, and the material is stabilized. Modulus K2 in terms of the heel length and the notch depth had almost the same and more transparent tendencies, as compared to modulus K1. Although it is worth noting that the confidence interval of the mean values was still considerable. The stiffness results were not more consistent after the first loading-unloading cycle. The loading speed was manually set for each specimen and constant in the loading sequences. This variable was massively varied but did not have any significant effect on the stiffness and the maximum load.



Figure 10. Screw uninstallation.

3.6. Influence of Moisture Content of Timber

The moisture content of timber was measured after the test, as it was considered as an essential variable. Some specimens showed minor color change spots and no significant deformations of the upmost timber layer. Most of the series had stiffness K1 reduced when the timber humidity increased (eight over 13 series). The same phenomenon could be observed in K2 (10 over 13 series) and Fmax (eight over 13 series). Only the correlations between stiffness K1 and moisture content are shown in Figure 11.

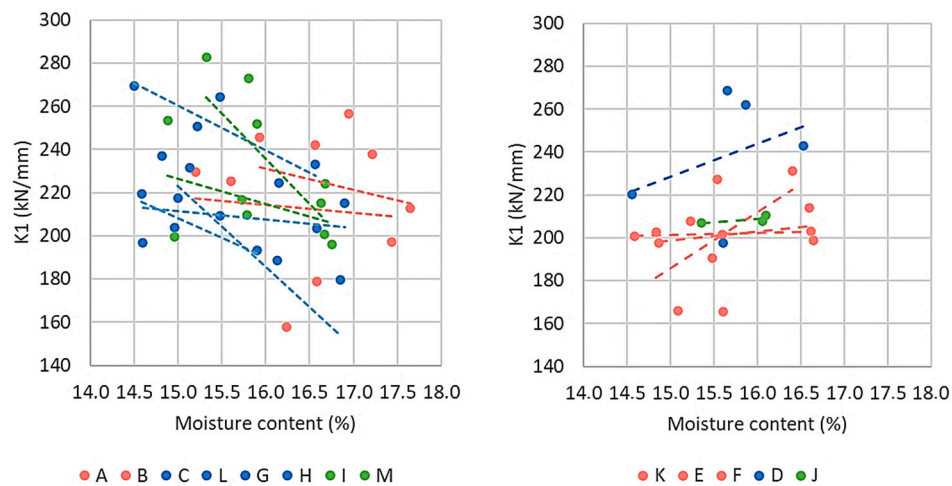


Figure 11. Correlation between stiffness K_1 and moisture content of timber of different series. 20 mm notch depth specimens are represented by the red points, 25 mm in green, and 35 mm in blue.

3.7. Failure Types

Three principal failure types were observed. Figure 12 shows the typical load-slip curves of different failure types. Figure 13 presents photos of these different failure types. Most of the tested specimens in this study had the failure type with a compression zone principally in the heel (47 over 60 tested samples). They were classified as type TD.

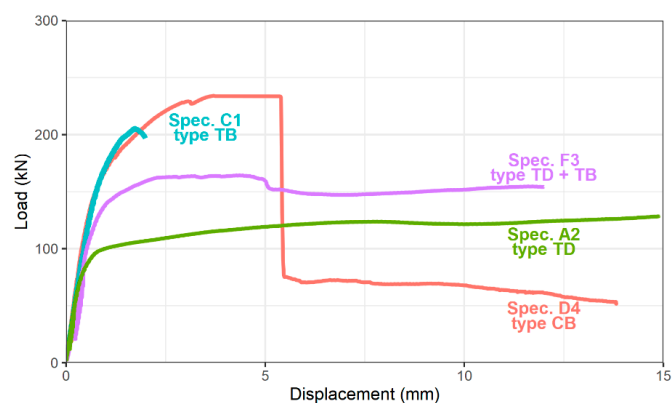


Figure 12. Load-slip curves of different failure types.

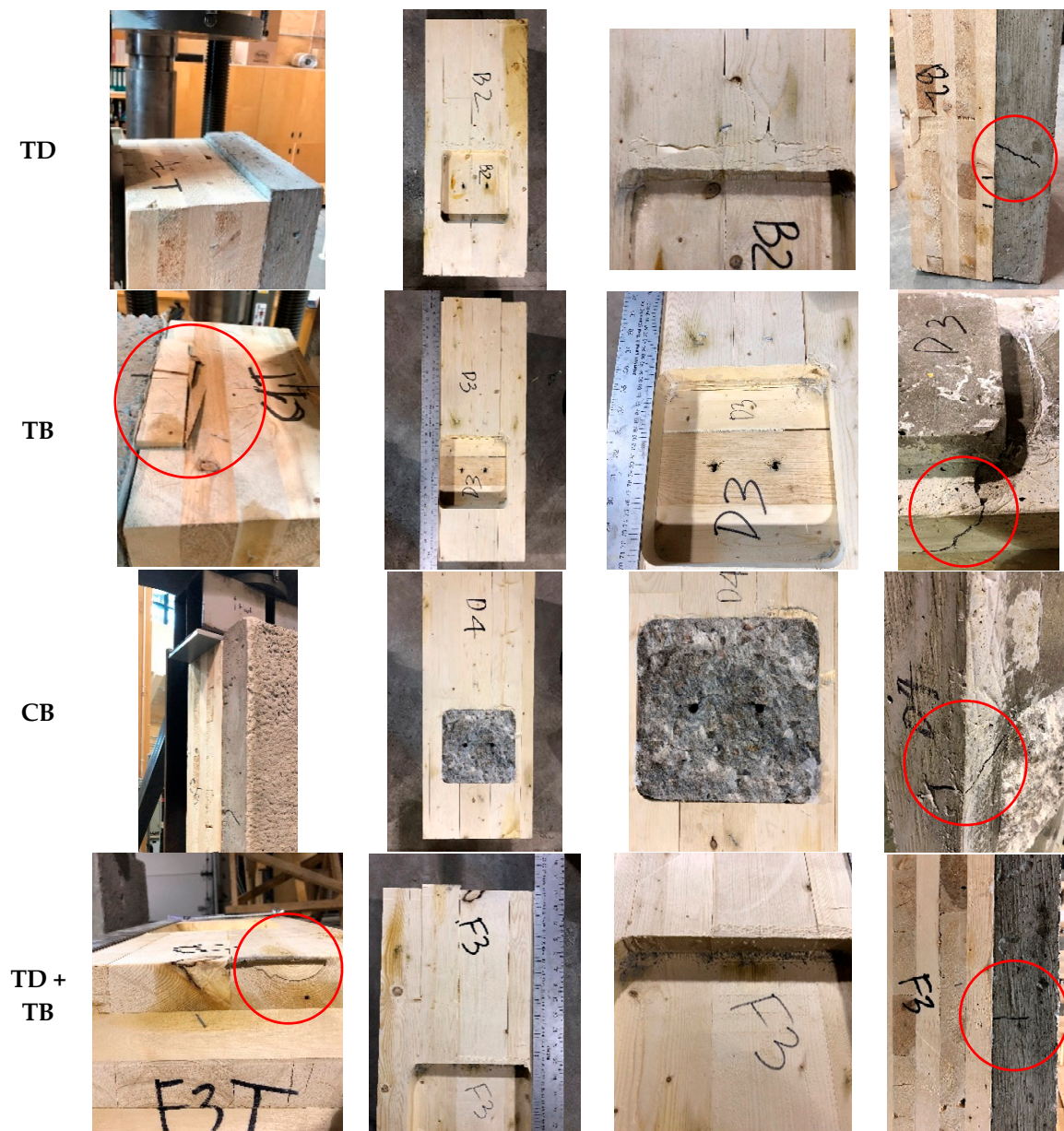


Figure 13. Typical different failure types.

The failure type TB occurred when the lamellas of the heel got sheared-off at the displacement from 2 mm to 3 mm. The full measured curves of type TB could reach a significant displacement at a relatively high load. This is because, firstly, when the testing machine pushed to the timber part, it held the sheared-off lamellas in place. The metal plate, designated for distributing the load from the testing machine, covered the surface of the timber upper part. When the timber lamellas of the heel part were sheared-off, the metal plate held the lamellas in place and caused a load increase in the load-displacement curve. Secondly, at a significant slip, only the screws bear the load. The sleeve between screws and concrete would prevent the contribution of the screws to the shear loading from initial up to 2 mm of displacement. Regarding this artifact, we considered that the specimen failed at the first drop in terms of load.

In the specimens classified as type TD + TB, there was a minor drop in the load after the sample reaches its peak load at the slip of about 2 mm to 6 mm. The specimens still were carrying on and achieved a significant displacement (10 mm or more) because there was a portion of the heel still glued

to the transversal layer, got crushed at the loaded edge, and held the charge. Hence, we considered this type as a sub-category of type TD.

In the specimens classified as type CB, the notched concrete part was sheared-off while the load was still increasing. After the failure, the screws held the residual charge. It is worth noting that the concrete has rebar steel mesh, and the two screws rigidly attached the two parts altogether. Therefore, the connector in this study was less likely to have the failure type CB (two over 60 specimens).

Almost every specimen had diagonal cracks at failure. These cracks took place in the corner between timber and concrete shortly before the load reaches its peak. They developed at an angle from 30° to 45° to the concrete's surface. A plastic hinge was observed in the screw at the interface location. However, this only contributed to the post-peak behavior and helped extend the slip. The reasons are, firstly, that an individual screw was much less rigid than the notch itself. Secondly, there was a gap between the screw and the concrete due to the plastic sleeve; it prevented the screw from contributing to the connector rigidity.

Figure 14 the failure types distribution for only one variable at a time; the data labels represent the number of specimens. The percentage of failure type TD reduced from 73% to 61% when the heel length decreased from 400 mm to 300 mm. The timber imperfection was likely to be manifested heavily by a brittle failure in the specimens with a shorter heel. In terms of notch depth, one could observe a significant reduction from 87% at 20 mm depth to 48% at 35 mm depth.

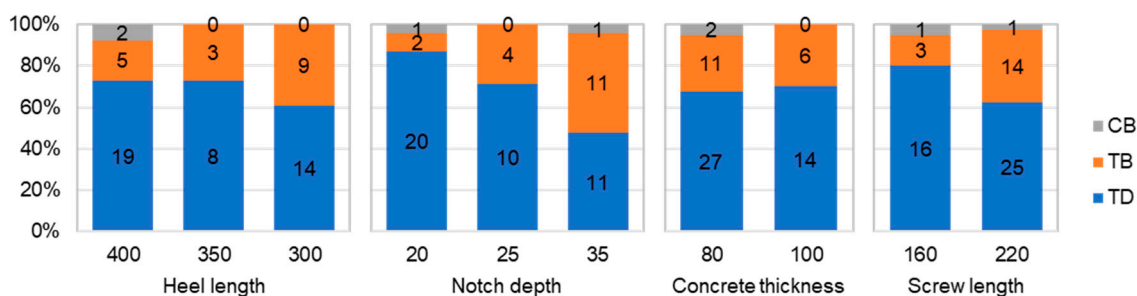


Figure 14. Number of specimens with different failure types.

The deeper notch must withstand greater shear force, and more likely failed in a brittle manner. This shows differences in load transmission depending on heel length and notch depth. As lamellas were not edgewise glued, the sheared area must be significant enough not to be the weakest (brittle) link versus the compressed (ductile) parallel-to-grain area. Potential future design rules will have to prevent brittle failure. One could see that the thickness of the concrete layer did not influence the distribution of failure type. The longer screw might have caused a brittle rupture of the connector, from 15% to 35% of the specimen's number (three over 20 specimens versus 14 over 40 specimens). Further investigation is needed to confirm this phenomenon.

4. Finite Elements Model Validation

Many authors have used different techniques to model timber material in terms of connection, whether for notched or dowel connectors. Dias et al. [29] used Hill's criterion to characterize the anisotropy of timber material. The method was useful in terms of modeling elastic-plastic behavior and was later employed in CCC by Jiang et al. [19] for notched connector and Mai et al. [16] for screw connectors. Models with damage mechanics were also adopted in the literature, such as using continuum damage mechanics to obtain brittle and ductile failure modes (Sandhaas and van de Kuilen [30]), using Hashin failure criterion for the laterally loaded nail of CLT bracket connection (Hollenbeck [31]), cohesive elements to simulate cracking in timber bolted connection (Franke and Quenneville [32]). User-defined features (such as subroutine in Abaqus) is required for such applications and raises concerns about the computational cost.

4.1. Materials

4.1.1. Timber

Timber was modeled as an orthotropic elastic-perfect plastic material. According to Dias et al. [29], Hill's criterion, which is an extension of von Mises's function, could be used for orthotropic material to characterize the yielding phenomenon:

$$f(\sigma) = F(\sigma_{22} - \sigma_{33})^2 + G(\sigma_{33} - \sigma_{11})^2 + H(\sigma_{11} - \sigma_{22})^2 + 2L\sigma_{23}^2 + 2M\sigma_{31}^2 + 2N\sigma_{12}^2 \quad (1)$$

where F , G , H , L , M , and N are constants determined experimentally:

$$F = \frac{(\sigma^0)^2}{2} \left(\frac{1}{\bar{\sigma}_{22}^2} + \frac{1}{\bar{\sigma}_{33}^2} - \frac{1}{\bar{\sigma}_{11}^2} \right); \quad (2)$$

$$G = \frac{(\sigma^0)^2}{2} \left(\frac{1}{\bar{\sigma}_{33}^2} + \frac{1}{\bar{\sigma}_{11}^2} - \frac{1}{\bar{\sigma}_{22}^2} \right); \quad (3)$$

$$H = \frac{(\sigma^0)^2}{2} \left(\frac{1}{\bar{\sigma}_{11}^2} + \frac{1}{\bar{\sigma}_{22}^2} - \frac{1}{\bar{\sigma}_{33}^2} \right); \quad (4)$$

$$L = \frac{3}{2} \left(\frac{\tau^0}{\bar{\sigma}_{23}} \right)^2; \quad (5)$$

$$M = \frac{3}{2} \left(\frac{\tau^0}{\bar{\sigma}_{13}} \right)^2; \quad (6)$$

$$N = \frac{3}{2} \left(\frac{\tau^0}{\bar{\sigma}_{12}} \right)^2. \quad (7)$$

The definition of the potential coefficients R_{ij} is:

$$R_{11}, R_{22}, R_{33}, R_{12}, R_{13}, R_{23} = \frac{\bar{\sigma}_{11}}{\sigma^0}, \frac{\bar{\sigma}_{22}}{\sigma^0}, \frac{\bar{\sigma}_{33}}{\sigma^0}, \frac{\bar{\sigma}_{12}}{\tau^0}, \frac{\bar{\sigma}_{13}}{\tau^0}, \frac{\bar{\sigma}_{23}}{\tau^0} \quad (8)$$

where $\bar{\sigma}_{ij}$ is the measured yield stress value when σ_{ij} is applied as the only nonzero stress component; σ^0 is the reference yield stress and $\tau^0 = \sigma^0 / \sqrt{3}$. The problem was defining the yield stress σ^0 and the yield stress ratio R_{ij} . Considering σ^0 as the yield strength in the direction parallel to the grain of the timber, Dias et al. [29] proposed the coefficients R_{ij} for spruce $R_{11} = 1; R_{22} = R_{33} = 0.19$ and $R_{12} = R_{13} = R_{23} = 0.38$. The Wood Handbook [33] suggests $R_{11} = 1; R_{22} = R_{33} = 0.11$ and $R_{12} = R_{13} = R_{23} = 0.39$ (mean value) for Canadian SPF. The model used value from this reference [33].

The preliminary modeling showed that the resistance of the notched connector depends heavily on the "shear" ratio R_{12}, R_{13} rather than the "orthogonal" ratio R_{22}, R_{33} . The lamellas of the third and fifth layers of CLT specimen were extracted and subjected to the compression tests, based on standard ASTM D143-2014 [34] for a small clear specimen of timber.

Table 4 presents the extreme case value of σ^0 and E_{xx} obtained from the experimental tests [35]. Other properties $E_{yy}, E_{zz}, G_{xy}, G_{zx}, G_{yz}$ were derived from E_{xx} as the indications of EN 338 [36] for softwoods:

$$E_{xx} = 30E_{yy} = 30E_{zz} \quad (9)$$

$$16G_{xy} = 16G_{xz} = 0.5(E_{xx} + E_{yy}) \quad (10)$$

$$16G_{yz} = 0.5(E_{yy} + E_{zz}) \quad (11)$$

Table 4. Summary of the timber parameters of the FEM model.

Parameters	Value	Parameters	Value	Parameters	Value
σ^0	37.5–25.8	E_{xx}	18200–9340	ν_{xy}	0.4
R_{11}	1	E_{yy}, E_{zz}	607–311	ν_{xz}	0.3
R_{22}, R_{33}	0.11	G_{xy}, G_{zx}	588–302	ν_{yz}	0.3
R_{12}, R_{13}, R_{23}	0.39	G_{yz}	59–30	(–)	(–)

4.1.2. Concrete

Concrete was modeled as an isotropic elastic material without any plasticity properties. The experimental test provided the modulus of elasticity of concrete (cf. Table 1). The impact of plasticity characteristics of concrete was considered minimal to the model based on preliminary modeling. This simplification helped reduce the computational cost and increased the possibility of convergence of the model.

4.2. Models

The finite element model of the notched connector was performed with the commercial software Abaqus [37]. The tie constraint was used for the glued contact between the lamellas (rigid contact). The non-glued one and the one between timber and concrete had “hard” contact in the normal direction and “frictionless” in the tangential direction. The finite elements were eight-node cubic with reduced integration C3D8R. The reduced integration minimized the computational effort but raised some problems in terms of “hourglass.” Hourglass is nonphysical, zero-energy modes of deformation that produce zero strain and no stress. This occurs in the reduced integration elements, with only 1 integration point in the middle (e.g., C3D8R). To minimize it, we used the default hourglass control algorithm of Abaqus. The fine mesh of 4 mm-element was applied to the contact zone of concrete and timber down to the second layer. The coarse mesh of 12 mm was for the rest of the model (Figure 14). The local failure criteria of the materials were not implemented. We imposed a criterion of global relative displacement of 10 mm between timber and concrete. Hill’s criteria were used for the sake of yielding phenomenon in orthotropic material, i.e., timber in our case.

The screws were omitted because of their minimal impact on the overall performances of the connector. Only half of the specimen was modeled to reduce the computational cost. The charge was placed on the concrete part. The boundary condition was set to imitate the behavior of the specimen on the bench test. The CLT part was limited in the translational displacement U_y and U_x , while the concrete part was constrained in the U_y of the loaded end (Figure 15). The model was built based on the standard/implicit calculation regime. Abaqus would check for the convergence of the model at each iteration. The convergence of the model was quite good for displacement from 0 to 4 mm. Beyond this, there were some cases where the model aborts the calculation due to the divergence. The excessive displacement of the element at the loaded edge of the notch might be the reason for this divergence.

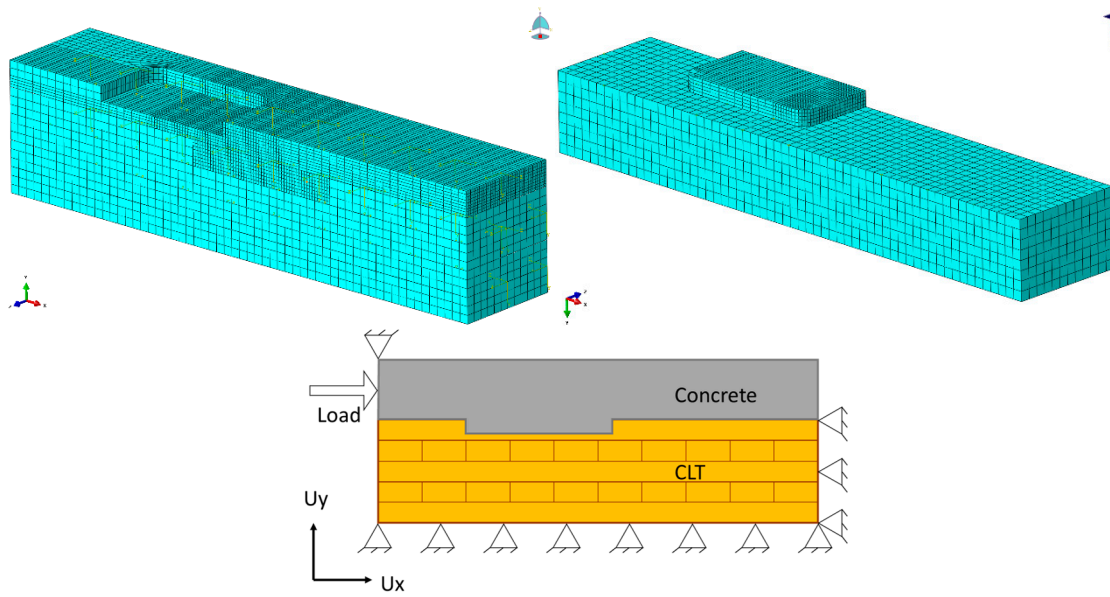


Figure 15. Mesh definition of timber and concrete part and boundary conditions.

4.3. Results

For the stiffness of the connector, the model could capture the trend in terms of notch depth. Figure 16 shows that the stiffness per depth decreases when the notch depth increase. The model yields a better prediction for K2 than for K1.

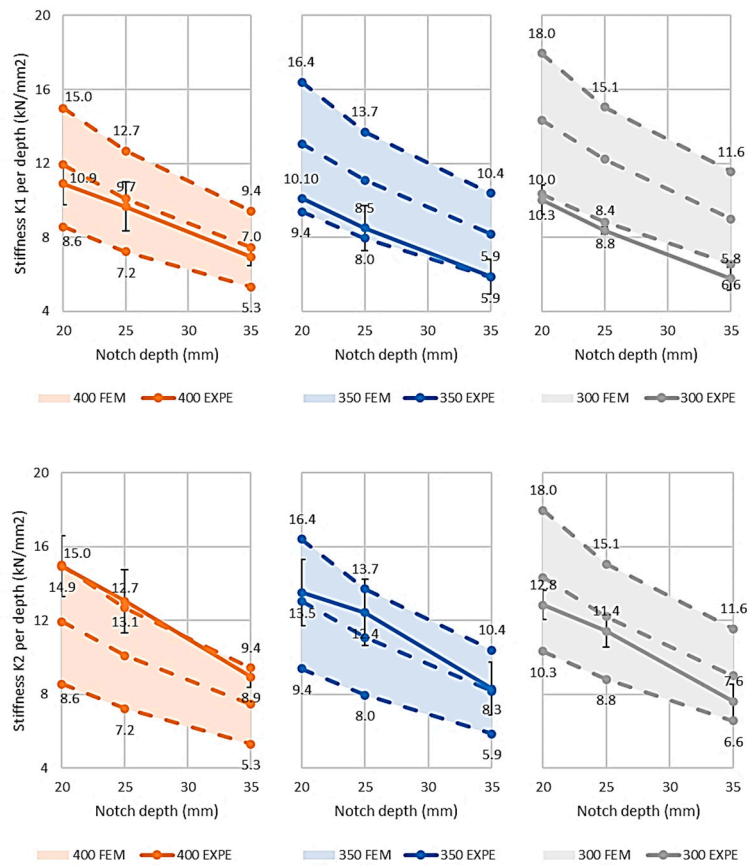


Figure 16. FEM envelop of stiffness K1 and K2 per depth of multiple heel length.

These results showed that the initial loading and the unloading step of the test might impact the specimen (close the contact and stabilize the material). However, it exhibited an opposite trend in terms of the heel length. The experimental stiffness (both K1 and K2) decreased for a smaller length; the stiffness of the model increases. It could be explained that our model assumed the same modulus of elasticity for both compression and traction behavior of timber.

For the maximum load, the model could characterize the trend in terms of notch depth and heel length (Figure 17). The envelope of maximum load created by the model was consistent in terms of heel length and increased when the depth of the cut is more profound. The model over-estimated the load even though we used the experimental compression data of lamellas of the tested CLT.

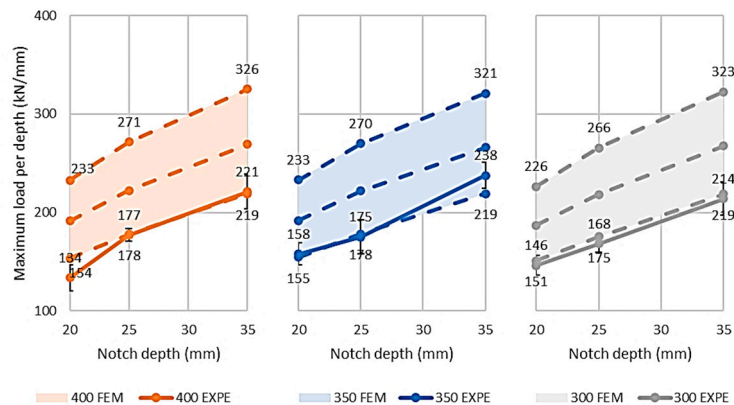


Figure 17. FEM envelop of maximum load F_{max} per notch depth.

The comparison between the experimental and modeled load-displacement curves of series I is shown in Figure 18. The model strength was overestimated when using the upper bound of the reference yield strength σ^0 (37.5 MPa, cf. Table 4) while it showed some agreement up to the displacement of 6 mm at lower strength bound (25.8 MPa).

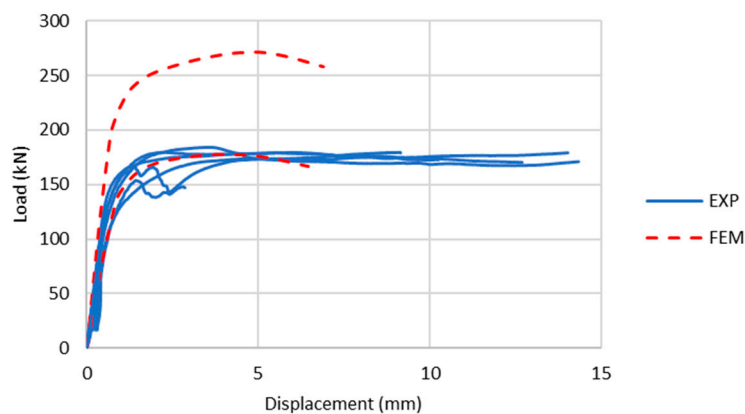


Figure 18. Load-displacement curves comparison between experimental and FEM of series I.

5. Conclusions

We have investigated and compared the influence of four variables on the overall mechanical performance of the notched connector. The variables tested were heel length, notch depth, screw length, and thickness of the concrete layer. The following conclusions were drawn from the results of the study:

- (1) Based on the load-displacement behavior of the specimens, the notched connector with reinforced screws could withstand a load from 120 kN to 240 kN. The resistance of connectors depended on

the geometry configuration. The stiffness of the notched connector was higher than the screw connectors but lower than HBV mesh. Most of the specimens exhibited ductile rupture with significant post-peak displacement.

- (2) By comparing the results of different configuration, the geometry variables, heel length, and notch depth had significant influences on the stiffness and the maximum load of the connector than other variables. The performance of the connector was not increased proportionally with a deeper notch cut. Screw length and concrete thickness only had minor influences that are difficult to spot since the number of tests was limited.
- (3) The finite element model could capture the tendency of both stiffness and maximum load in terms of notch depth. For a better prediction of stiffness, the model would need to characterize different timber modulus of elasticity for compression and traction. Such implementation requires user-coded material in Abaqus, which is out of the scope of this study.
- (4) The results showed that the length of the screw did not impact the overall results. After the test, the specimens were successfully disassembled and separated by using a simple screwdriver. This connector system could be employed if there are concerns about the reusability at the end of the structure service life.

This study gave more information about the performance of individual notched connectors of different geometry configurations. The finite-element model could produce a reasonably good prediction, though, it could not entirely capture the experimental phenomenon due to an over-simplified timber material. Since our next step would focus on the vibrational behavior of full-scale specimens, this study provided a basis to create a simplified parametrical model of the connector for a global optimization application. For future research, full-scale testing of long-span CCC beams will adopt this type of connector. The presented findings on individual behavior (strength, stiffness) and many other aspects such as group effect, number of connectors, the distance between the connectors will be considered. One of the objectives of our research project is to propose a solution to a deconstructable connector. It involved a vision at the scale of beams, floors, and entire structures. This solution will also be validated in-depth on a full-scale beam test.

Author Contributions: Methodology, M.V.T., and P.G.; validation, M.V.T.; investigation, M.V.T.; data curation, M.V.T.; writing—original draft preparation, M.V.T.; writing—review and editing, M.V.T., S.M., S.M.E., and P.G.; visualization, M.V.T.; supervision, S.M., and S.M.E.; funding acquisition, S.M. All authors have read and agreed to the published version of the manuscript.

Funding: The authors are grateful to Natural Sciences and Engineering Research Council of Canada for the financial support through its IRC and CRD programs (IRCPJ 461745-18 and RDCPJ 524504-18) as well as the industrial partners of the NSERC industrial chair on eco-responsible wood construction (CIRCERB).

Conflicts of Interest: The authors declare no conflict of interest.

References

1. Gauthier, P.-E. Charpente en Bois, Notamment Pour Ossature de Hangar Agricole. 1952. Available online: <https://bases-brevets.inpi.fr/fr/document/FR1009171/publications.html> (accessed on 7 July 2020).
2. Karacabeyli, E.; Gagnon, S. (Eds.) *Canadian CLT Handbook*, 2019th ed.; Special Publication SP-532E; FPInnovations: Point-Claire, QC, Canada, 2019; ISBN 978-0-86488-590-6.
3. Lukaszewska, E. Development of Prefabricated Timber-Concrete Composite Floors. Ph.D. Thesis, Luleå University of Technology, Luleå, Sweden, 2009.
4. Dias, A.M.P.G.; Jorge, L. The effect of ductile connectors on the behaviour of timber–concrete composite beams. *Eng. Struct.* **2011**, *33*, 3033–3042. [[CrossRef](#)]
5. Fragiacommo, M.; Lukaszewska, E. Time-dependent behaviour of timber–concrete composite floors with prefabricated concrete slabs. *Eng. Struct.* **2013**, *52*, 687–696. [[CrossRef](#)]
6. Fragiacommo, M.; Amadio, C.; Macorini, L. Short- and long-term performance of the “Tecnaria” stud connector for timber-concrete composite beams. *Mater. Struct.* **2006**, *40*, 1013–1026. [[CrossRef](#)]

7. Frangi, A.; Knobloch, M.; Fontana, M. Fire Design of Timber-Concrete Composite Slabs with Screwed Connections. *J. Struct. Eng.* **2010**, *136*, 219–228. [[CrossRef](#)]
8. Yeoh, D.; Fragiaco, M.; Buchanan, A.; Gerber, C. Preliminary Research Towards A Semi-Prefabricated LVL—Concrete Composite Floor System for the Australasian Market. *Aust. J. Struct. Eng.* **2009**, *9*, 225–240. [[CrossRef](#)]
9. WoodWorks Case Study: Inspiration through Innovation at UMass Amherst, an Exposed Mass Timber Structure is a Teaching Tool. Available online: <http://www.woodworks.org/wp-content/uploads/UMass-Amherst-Olver-Design-Building-WoodWorks-Case-Study.pdf> (accessed on 7 July 2020).
10. Ceccotti, A. Composite concrete-timber structures. *Prog. Struct. Eng. Mater.* **2002**, *4*, 264–275. [[CrossRef](#)]
11. Lukaszewska, E.; Johnsson, H.; Fragiaco, M. Performance of connections for prefabricated timber–concrete composite floors. *Mater. Struct.* **2008**, *41*, 1533–1550. [[CrossRef](#)]
12. Van der Linden, M. *Timber-Concrete Composite Floor Systems*; University of Technology Delft: Delft, The Netherlands, 1999.
13. Yeoh, D.; Fragiaco, M.; Aldi, P.; Mazzilli, M.; Kuhlmann, U. Performance of Notched Coach Screw Connection for Timber-Concrete Composite Floor System. In Proceedings of the 10th World Conference on Timber Engineering, Miyazaki, Japan, 2–5 June 2008; paper 221. pp. 1–8.
14. Dias, A.M.P.G.; Cruz, H.M.P.; Lopes, S.M.R.; Van De Kuilen, J.W. Stiffness of dowel-type fasteners in timber–concrete joints. *Struct. Build.* **2010**, *163*, 257–266. [[CrossRef](#)]
15. Gerber, A.R. Timber-Concrete Composite Connectors in Flat-Plate Engineered Wood Products. Master’s Thesis, University of British Columbia, Vancouver, BC, Canada, 2016.
16. Mai, K.Q.; Park, A.; Lee, K. Experimental and numerical performance of shear connections in CLT–concrete composite floor. *Mater. Struct.* **2018**, *51*, 84. [[CrossRef](#)]
17. Mai, K.Q.; Park, A.; Nguyen, K.T.; Lee, K. Full-scale static and dynamic experiments of hybrid CLT–concrete composite floor. *Constr. Build. Mater.* **2018**, *170*, 55–65. [[CrossRef](#)]
18. Higgins, C.; Barbosa, A.R.; Blank, C. *Structural Tests of Concrete Composite-Cross-Laminated Timber Floors*; School of Civil and Construction Engineering: Corvallis, OR, USA, 2017; p. 76.
19. Jiang, Y.; Crocetti, R. CLT-concrete composite floors with notched shear connectors. *Constr. Build. Mater.* **2019**, *195*, 127–139. [[CrossRef](#)]
20. Khorsandnia, N.; Valipour, H.; Schänzlin, J.; Crews, K. Experimental Investigations of Deconstructable Timber–Concrete Composite Beams. *J. Struct. Eng.* **2016**, *142*, 04016130. [[CrossRef](#)]
21. *ANSI/APA PRG-320-2019 Standard for Performance-Rated Cross-Laminated Timber*; APA—The Engineered Wood Association: Tacoma, WA, USA, 2019.
22. *NRC—CNRC Evaluation Listing CCMC 13654-L Nordic X-Lam*; National Research Council of Canada: Ottawa, ON, Canada, 2013.
23. *ASTM C39/C39M—18 Test Method for Compressive Strength of Cylindrical Concrete Specimens*; ASTM C39/C39M—18; ASTM International: West Conshohocken, PA, USA, 2018.
24. Boccadoro, L. Timber-Concrete Composite Slabs Made of Beech Laminated Veneer Lumber with Notched Connection. Ph.D. Thesis, ETH Zurich, Zürich, Switzerland, 2016.
25. Gutkowski, R.M.; Brown, K.; Shigidi, A.; Natterer, J. Investigation of Notched Composite Wood–Concrete Connections. *J. Struct. Eng.* **2004**, *130*, 1553–1561. [[CrossRef](#)]
26. *EN 26891: 1991 Timber Structures: Joints Made with Mechanical Fasteners: General Principles for the Determination of Strength and Deformation Characteristics*; EN 26891:1991; European Committee for Standardization (CEN): Brussels, Belgium, 1991; ISBN 978-0-580-19856-4.
27. *MyTiCon Structural Screw Design Guide*; MyTiCon Timber Connectors: Surrey, BC, Canada, 2020.
28. *TiComTec Technical Dossier—HBV Systems*; TiComTec: Haibach, Germany, 2014.
29. Dias, A.M.P.G.; Van De Kuilen, J.-W.G.; Lopes, S.M.R.; Cruz, H. A non-linear 3D FEM model to simulate timber–concrete joints. *Adv. Eng. Softw.* **2007**, *38*, 522–530. [[CrossRef](#)]
30. Sandhaas, C.; van de Kuilen, J.W.G. Material model for wood. *HERON* **2013**, *58*, 179–199.
31. Hollenbeck, S. Numerical Modeling of Mass Timber Connections. Master’s Thesis, Oregon State University, Corvallis, OR, USA, 2018.
32. Franke, B.; Quenneville, P. Numerical Modeling of the Failure Behavior of Dowel Connections in Wood. *J. Eng. Mech.* **2011**, *137*, 186–195. [[CrossRef](#)]

33. Laboratory, F.P. *Wood Handbook: Wood as an Engineering Material*; USDA Forest Service: Madison, WI, USA, 1999; Volume 113, p. 509.
34. *ASTM D143—14 Test Methods for Small Clear Specimens of Timber*; ASTM International: West Conshohocken, PA, USA, 2014.
35. Thai, M.V.; Ménard, S.; Elachachi, S.M.; Galimard, P. *Experimental Report on the Push-Out Test of CLT-Concrete Shear Notched Connector (Phase 1)*; University of Bordeaux: Bordeaux, France, 2019.
36. *EN 338—2009 Structural Timber—Strength Classes*; European Committee for Standardization (CEN): Brussels, Belgium, 2009.
37. *Abaqus 6.14 Online Documentation*; Dassault Systèmes: Velizy-Villacoublay, France, 2014; Available online: <http://ivt-abaqusdoc.ivt.ntnu.no:2080/v6.14/books/usb/default.htm> (accessed on 7 July 2020).



© 2020 by the authors. Licensee MDPI, Basel, Switzerland. This article is an open access article distributed under the terms and conditions of the Creative Commons Attribution (CC BY) license (<http://creativecommons.org/licenses/by/4.0/>).